Experimental Eye Research 128 (2014) 1–7

Contents lists available at ScienceDirect

Experimental Eye Research

journal homepage: www.elsevier.com/locate/yexer

Application of Elliptic Fourier analysis to describe the lamina cribrosa shape with age and intraocular pressure

P.G. Sanfilippo [e], J.L. Grimm [a], J.G. Flanagan [c, d], K.L. Lathrop [a, b], I.A. Sigal [a, b, *]

[a] Department of Ophthalmology, University of Pittsburgh, Pittsburgh, PA, USA
[b] Department of Bioengineering, University of Pittsburgh, Pittsburgh, PA, USA
[c] Department of Ophthalmology and Vision Science, University of Toronto, Toronto, ON, Canada
[d] School of Optometry and Vision Science, University of Waterloo, Waterloo, ON, Canada
[e] Centre for Eye Research Australia, Royal Victorian Eye and Ear Hospital, University of Melbourne, Melbourne, Australia

ARTICLE INFO

Article history:
Received 15 May 2014
Accepted in revised form 22 August 2014
Available online 2 September 2014

Keywords:
optic nerve head
lamina cribrosa
morphometry
glaucoma

ABSTRACT

The lamina cribrosa (LC) plays an important biomechanical role in the optic nerve head (ONH). We developed a statistical shape model of the LC and tested if the shape varies with age or IOP. The ONHs of 18 donor eyes (47–91 years, mean 76 years) fixed at either 5 or 50 mmHg of IOP were sectioned, stained, and imaged under a microscope. A 3D model of each ONH was reconstructed and the outline of the vertical sagittal section closest to the geometric center of the LC extracted. The outline shape was described using Elliptic Fourier analysis, and principal components analysis (PCA) employed to identify the primary modes of LC shape variation. Linear mixed effect models were used to determine if the shape measurements were associated with age or IOP. The analysis revealed several modes of shape variation: thickness and depth directly (PC 1), or inversely (PC 2) related, and superior–inferior asymmetry (PC 3). Only PC 3 was associated with IOP, with higher IOP correlating with greater curvature of the LC superiorly compared to inferiorly. Our analysis enabled a concise and complete characterization of LC shape, revealing variations without defining them *a priori*. No association between LC shape and age was found for the relatively old population studied. Superior–inferior asymmetry of LC shape was associated with IOP, with more asymmetry at higher IOP. Increased IOP was not associated with LC thickness or depth.

1. Introduction

The characteristic morphological changes of the optic nerve head (ONH) that occur concurrently with glaucoma have long been regarded as an important clinical biomarker of disease progression. Mounting evidence suggests that injury to the retinal ganglion cell axons at the level of the lamina cribrosa (LC) causes the surface morphology changes associated with ONH cupping and the ensuing vision loss (Quigley and Cone, 2013).

The LC is shaped by the spatial distribution of dense collagenous trabeculae that provide structural and nutritional support to the ganglion cell axons within the anterior region of the scleral canal (Sigal and Ethier, 2009). Numerous studies have focused on the analysis of LC shape, hypothesizing that this might represent a biomarker useful for glaucoma, for example: i) LC shape could indicate the strength of the tissues to resist the biomechanical insult of elevated IOP, e.g. thicker LCs corresponding with stiffer, stronger LCs (Sigal et al., 2005a; Yang et al., 2009), ii) LC shape may mark progression of glaucomatous neuropathy, e.g. thinner LCs corresponding with more advanced disease (Ren et al., 2009), perhaps with thickened LCs early in the disease (Yang et al., 2007), iii) changes in LC shape could indicate the sensitivity to IOP, e.g. LCs that deform more under elevated IOP corresponding with increased sensitivity to IOP (Yang et al., 2007; Grytz et al., 2012). However, there is no standardized method for measuring and describing the LC shape. A robust method of characterizing LC shape would enable a more refined description and comprehensive understanding of regional anatomy, sensitivity to IOP and progression of disease.

LC shape has conventionally been described using the so-called 'traditional morphometrics' (Quigley et al., 1990; Jonas et al., 1991). These methods, however, bear significant limitations including low statistical power due to measurement collinearity and the requirement that features of interest be defined *a priori*. In order to

* Corresponding author. Laboratory of Ocular Biomechanics, Department of Ophthalmology, University of Pittsburgh, Medical Center, Eye & Ear Institute, 203 Lothrop St. Rm. 930, Pittsburgh, PA 15213, USA. Tel.: +1 412 864 2220; fax: +1 412 647 5880.
E-mail addresses: sigalia@upmc.edu, ian.sigal@gmail.com (I.A. Sigal).
URL: http://www.ocularbiomechanics.org

http://dx.doi.org/10.1016/j.exer.2014.08.013
0014-4835/

Fig. 1. Example of the LC section (left) and with the tissue segmentation overlaid (right). Five tissue regions were identified: pre and postlaminar neural tissue (yellow), LC (red), pia mater (green) and sclera (orange). The fiducial markers used for unwarping are the four dark dots. Segmentation was done using a combination of bright field (left) and dark field images (not shown).

circumvent these restrictions we developed a statistical model of the shape of the LC using the Elliptic Fourier analysis (EFA), a geometric morphometric technique that is commonly employed in the quantitative description of biological forms (Sanfilippo et al., 2009). The objective of this work was to characterize the shape of the LC and how it varies with IOP and age. We wanted to avoid preconceptions on the nature of the changes that would occur with age and IOP and therefore we used methods of geometric morphometrics that would help us find the changes in shape, rather than the methods of traditional morphometry.

2. Materials and methods

2.1. Eye and section preparation

Eighteen eyes from nine donors were obtained from the Eye Bank of Canada and managed in accordance with the provisions of the Declaration of Helsinki for research involving human tissue. A full description of the histologic techniques has been presented elsewhere (Sigal et al., 2010, 2012). Briefly, the eyes were perfusion fixed by rapidly exchanging the isotonic saline with fixative (2.5% paraformaldehyde/2.5% glutaraldehyde) and maintaining IOP for 24 h. In each set of eyes, one was fixed at 5 mmHg, and the other at 50 mmHg. After fixation the ONH and peripapillary sclera were embedded in JB-4 plastic using a special mold with collagen sutures as fiducial markers. Sagittal (superior–inferior) sections 2 μm thick were cut at right angles to the fiducial markers. Sections were then stained with picrosirius red to identify collagen, and solochrome cyanin to identify myelin, nuclei, and blood cells, and photographed under bright field and dark field illumination (Leica MZ6, Heerbrugg, Switzerland) using a Nikon Coolpix 990 digital camera (2048 × 1536 pixels, 8 RGB bits per channel per pixel; Nikon, Tokyo, Japan). The images were aligned and unwarped to correct deformations that occurred during the sectioning process using a custom modified version of TPSSuper (F. James Rohlf, SUNY, Stony Brook, NY) based on the known fiducial marker positions as cast into the histologic block during the embedding procedure. From the images a 3D model of the ONH was reconstructed following our iterative procedure described elsewhere (Sigal et al., 2010). The anterior boundary of the LC was defined by the termination of the laminar beams and the insertion points at the sclera, whereas the posterior boundary was defined by two features: the termination of solochrome cyanin staining, indicating a lack of myelination inside the LC, and the "stacked plate" morphology of the connective tissues typical of the LC. To ensure consistency across all eyes, all the segmentations were checked and adjusted by a single observer (JGF). Once a 3D model of the ONH had been reconstructed and optimized, as described elsewhere (Sigal et al., 2010) the sagittal section closest to the center of mass of the 3D LC geometric center was selected and its segmentation used to define the LC for analysis for that eye. If the section contained the central retinal artery or vein through the LC the neighboring more temporal section was selected. This only occurred in four cases. Orientation information was preserved using the fiducial markers from the mold (Fig. 1).

2.2. Measurement of LC shape

EFA was used to quantify the shape of each LC section (Kuhl, 1982). With EFA, coefficients of sine and cosine terms

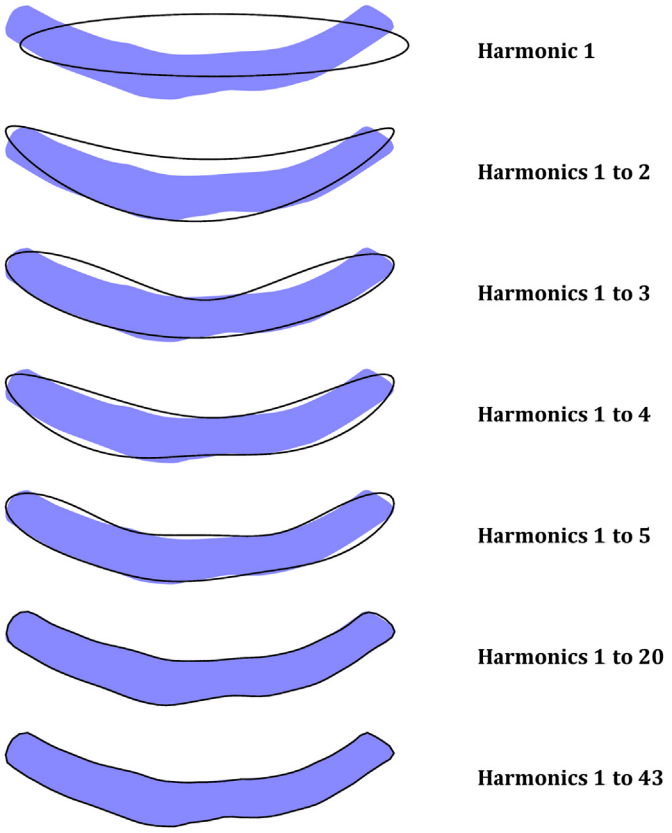

Fig. 2. Sequence of outline reconstructions from Elliptic Fourier analysis applied to the outline coordinates of the LC. The LC shape to be described is shown by the light blue shape, while reconstructed shapes are thin black outlines. Outlines are reconstructed using progressively more harmonics, from the simplest ellipse (one harmonic) at the top, to the highly accurate reconstructions with 20 and 43 harmonics. Note that each harmonic is described by four Fourier coefficients, two for the horizontal axis and two for the vertical axis.

(harmonics) are computed that may be used to reconstruct any set of consecutive, randomly spaced points that describe an outline of interest. While the number of harmonics available for the parameterization is theoretically infinite, a set can be found beyond which the contributions from additional harmonics are smaller than a given "accuracy" of the reconstruction (Fig. 2). Further, the number of harmonics is constrained by the number of points (or semi-landmarks) used to discretize the shape outline. For this study we set the number of harmonics at 43, which was consistent with the use of 100 points to describe the LC outlines, and permitted a reconstruction with 6 μm accuracy (appropriate to the reproducibility of our manual delineations) (Sigal et al., 2010). EFA utilizes a parametric description of curves in which the *x* and *y* coordinates of points represent functions of parameterized position along the curve from an arbitrary starting point. Each harmonic is described by four Fourier coefficients. The first harmonic was used to align the LC outlines and eliminate morphological variation unrelated to shape (i.e. location, orientation and size). As a result of this normalization procedure, the first three coefficients (out of 172) become redundant and were subsequently discarded. Principal component (PC) analysis of the remaining (169) harmonic coefficients was then employed as a dimensionality reduction technique to identify the main modes of shape variation (Sigal and Grimm, 2012). The first PC represents the greatest amount of variation in the dataset, with each successive component accounting for progressively less of the remainder. The effect of each PC on LC shape was visualized by allowing the score for a particular PC to equal the mean ± 2 standard deviations (SD), while keeping the scores of the remaining PCs equal to the mean. The shape changes associated with a particular PC were interpreted by visual inspection and according to our experience in LC morphology (Sigal et al., 2010, 2012). We also computed the error, defined as the mean distance between an outline and its representation with a given number of harmonics and PCs.

2.3. Validation on synthetic LCs

To test that EFA adequately captures LC shape and its variations, and that the results of the shape variation analysis are properly interpreted, we first analyzed a set of 143 synthetic (simulated) LCs with simple and known shape variations. These LCs were produced using the same mechanisms to generate LC shapes by which we have previously studied ONH biomechanics (Sigal et al., 2004, 2005a), except that for this work we only produced the LCs for shape analysis and did not require numerical modeling. Also, whereas in previous studies the LCs were axisymmetric, in this study we allowed asymmetry in LC thickness. Six variations were allowed in the set of LCs that we simulated: LC diameter, anterior–posterior position of the central LC, thickness at the center, angle of the canal wall, position asymmetry and thickness asymmetry. These last two parameters were ratios of the LC position and thickness on one side relative to the center. The other side was set to the inverse value, such that if one side was thicker or deeper than the center, the other side was thinner or shallower, and vice-versa. The parameter space was sampled according to a response surface analysis sampling scheme requiring 143 LCs (Sigal, 2011). EFA was then used to compute a matrix of shape variables and PC analysis performed to characterize the shape variation present. Optimally, the main modes of shape variation elicited should correspond to those defined *a priori*, thus indicating that EFA is a suitable technique for describing and quantifying differences in LC shape. In other words, the PCs should correspond with the known specific shape variations in the synthetic LCs.

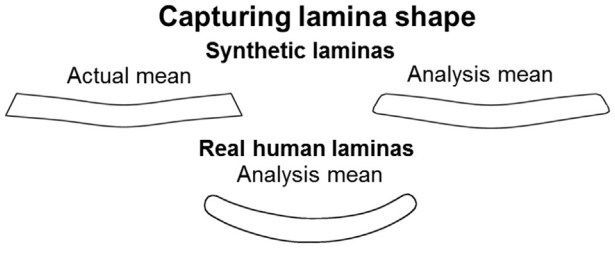

Fig. 3. Overall LC shape was well approximated. The error depended on the number of harmonics and principal components used. For example, for in real LCs the average errors were 4.8 μm, 1.6 μm and 0.7 μm, when using 17, 12 and 6 principal components, respectively, and 43 harmonics. Increasing the number of harmonics did not substantially reduce the error (less than 1 μm improvement for double the number of harmonics). For the synthetic LCs using 43 harmonics and 6 PCs resulted in an average error of 1.3 μm, mostly evident in the sharp corners of the LC insertion into the canal walls.

2.4. Application to real LCs

To test our main hypothesis that LC shape varies in response to IOP, we analyzed a set of 18 LC outlines obtained from histological sections of the ONH of normal human eyes 47–91 years (mean 76 yrs, SD 12 yrs). EFA and PCA were performed to summarize the main features of shape variation in the data.

2.5. Morphometric and statistical analyses

Morphometric analysis was performed using custom functions written in R to compute a series of Fourier coefficients representing LC shape (Claude, 2008). Subsequent analyses to evaluate shape variation (PCA) and associations were also conducted in the R statistical environment (R Development Core Team). Mixed-effects linear models were used to account for the non-independence of right and left eye data and to investigate potential associations between age, IOP and LC shape. For each PC, four models were evaluated with the following terms used as predictor variables for shape: (1) age, (2) IOP, (3) age and IOP and (4) age, IOP and an interaction between age and IOP. The Akaike information criterion (AIC) was used to determine the best-fitting model by evaluating model parsimony (i.e. the best goodness-of-fit combined with the fewest latent variables). The model with the lowest AIC suggests the best fit.

3. Results

EFA captured and described the synthetic LC shapes accurately as reflected by the small distance between actual and reconstructed outlines (average error 1.3 μm using 43 harmonics and 6 PCs) (Fig. 3). In addition, the PCs of the synthetic LCs matched those defined *a priori* in that the characteristics of shape variation interpreted from PCA corresponded to the modes simulated computationally.

3.1. Characteristics of LC shape

For the synthetic LCs, 64% of the overall variance was explained by the first PC and over 99% by the first six PCs (Fig. 4a). For the real LC data, 44% of the variation in the shape variables was explained by the first PC and 97% by the first six PCs (Fig. 4b). The remaining PCs were disregarded as the corresponding shape changes were smaller than what could be accounted for by our use of 100 points to describe the shape. The mean shape of the real LCs used in our study was found to be symmetric.

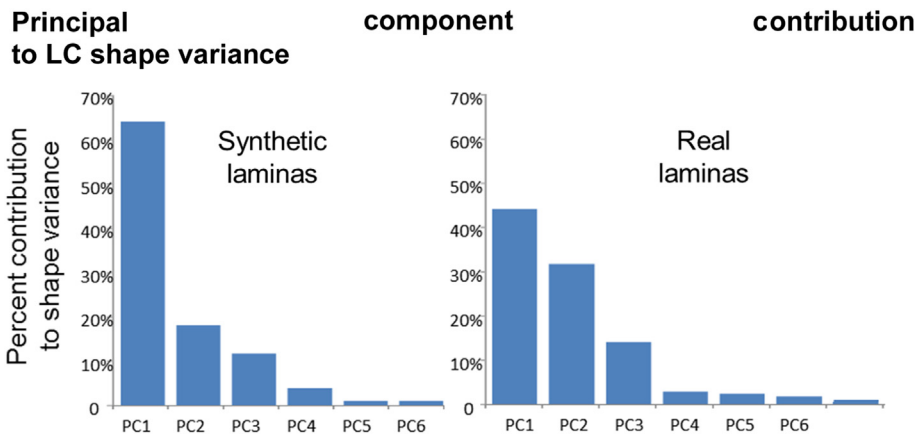

Fig. 4. The top six principal components, or modes of variation, accounted for 99% and 97% of shape variance in synthetic (left) and real (right) LCs, respectively.

The shape changes associated with the first six PCs of both the synthetic (a) and real (b) LCs were similar and are shown in Fig. 5. Several facets of shape variation are readily observable with the primary shape characteristic (PC 1: Thick and Deep) being symmetrical differences in LC thickness and depth. A positive score on this component represents a LC that is relatively thick and deep (at the center compared to periphery) and conversely, a negative score suggests that the LC is both thinner and shallower relative to the mean shape. The second PC (PC 2: Thick and Shallow) accounted for approximately 18% (synthetic), 32% (real) of the overall variation in LC shape and similarly with PC 1 describes differences in LC thickness and depth. However, in this shape dimension a positive score indicates a LC that is relatively thick and shallow compared to a thinner, deeper LC with a negative score on this axis. For both the synthetic and real LCs, these first two PCs describe similar shape features of the LC and taken together account for the vast majority of the total variance in the data (~82% synthetic, ~76% real).

The third PC (PC 3: Sup–Inf Asymmetry) explained approximately 12% (synthetic), 14% (real) of the overall shape variation and may be interpreted as asymmetry in LC shape (thickness and curvature) along the superior–inferior axis. For the synthetic LCs, the asymmetrical variation is predominantly in the posterior wall of the LC and manifests as differences in thickness; a positive score representing LC thinning superiorly and vice versa when the score is negative. In contrast, the gross asymmetry visualized for the real LCs may be attributed more to variation in LC curvature; in this case a more positive score reflecting greater curvature of the LC inferiorly compared to superiorly when a specimen shows a negative score along this dimension.

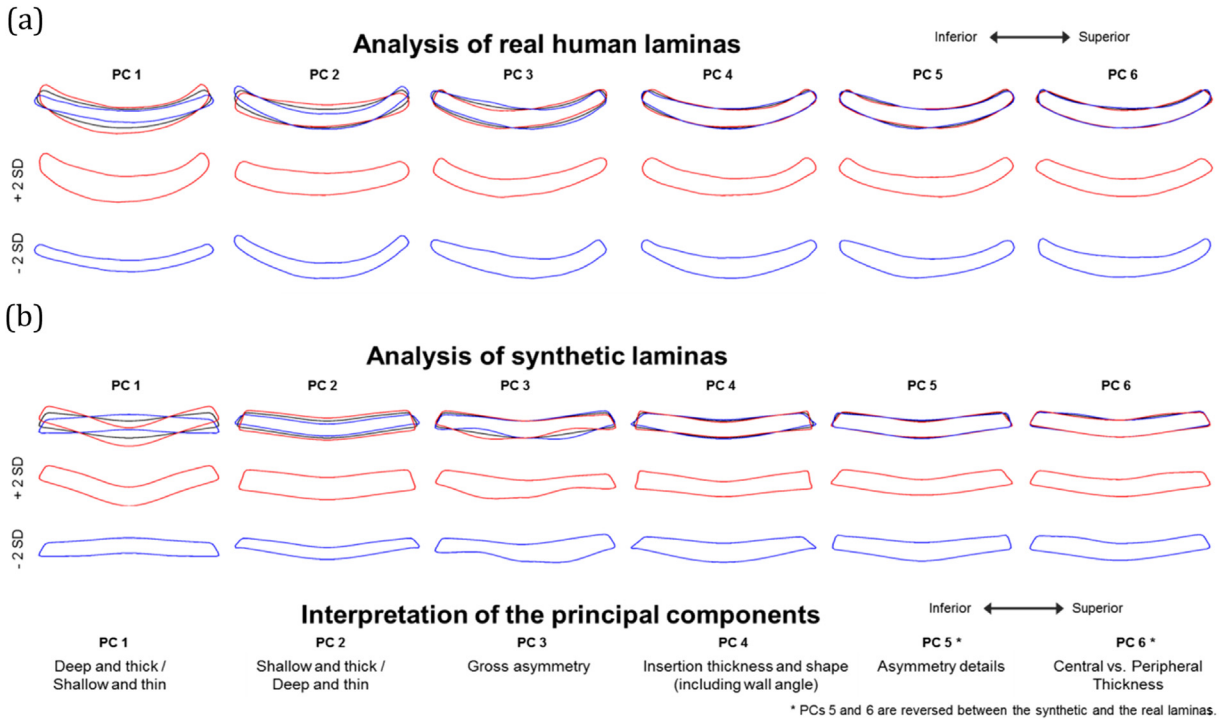

Fig. 5. The modes of variation in LC shape associated with the top 6 PCs of the real (a) and synthetic (b) LCs in our data. The top six principal components (PCs) representing the modes of variation in LC shape. The outlines represent the mean LC shape (black), +2 standard deviations (red) or −2 standard deviations (blue) for that PC. To simplify interpretation the outlines are shown overlaid on the mean (top rows) and independently (second and third rows). Note that the orientation, and thus the sign of a PCA axis is arbitrary. PCs reflect variation along an axis in multivariate space and do not have inherent direction. We describe the sign of the PC only to assist in the interpretation of the figures.

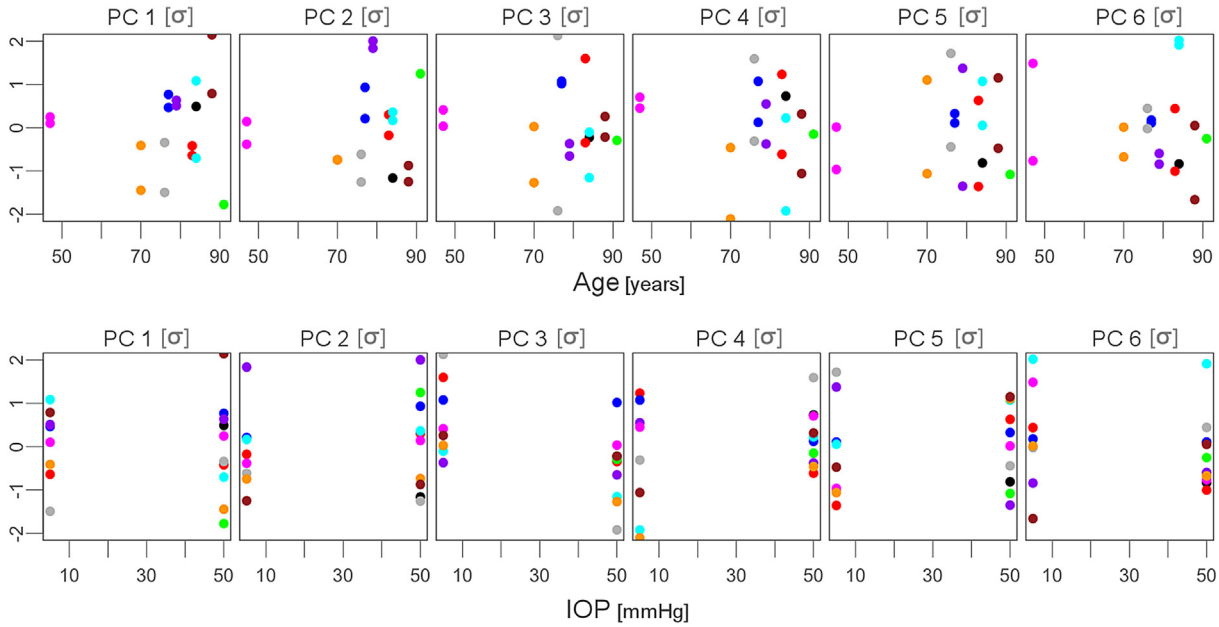

Fig. 6. Scatterplots of PCs (in standard deviations) vs. Age (y, top row) or IOP (mmHg, bottom row). Each dot represents an eye with contralateral eyes shown in the same color. Only PC 3 was significantly associated with IOP, and no PC was significantly associated with age. This can be distinguished in that in the plot of PC 3 vs. IOP the points at low IOP are generally higher than the points at high IOP. No clear trend is observed in other plots. See Table 1 for full statistical results.

The remaining PCs accounted for progressively less of the residual shape variation in the synthetic and real LC data sets. These shape features are illustrated graphically in Fig. 5; briefly, PC 4 describes variation in LC thickness at its insertion with the sclera (including the wall angle), and for the real LCs PC 5 may be interpreted as localized asymmetrical variation and PC 6 as differences in central compared to peripheral LC thickness. While the modes of shape variation are consistent across synthetic and real LC datasets for the first four PCs, those described by PCs 5 and 6 are swapped.

3.2. Association of LC shape with IOP and age

Scatterplots of real LC PC scores plotted against age and IOP are presented in Fig. 6. Table 1 shows the results of modeling age and IOP with LC shape. In general, LC shape was mostly independent of age or IOP, combinations of the variables or the interaction between them. One model (a mixed-effect model with IOP as predictor) did show a significant effect of IOP on one feature of LC shape (PC 3, superior–inferior asymmetry) and was the best-fitting model evaluated for that PC. In this case, the effect of increasing IOP appears to increase the curvature of the LC superiorly and/or decrease the curvature inferiorly along the central vertical axis. The shape characteristic described by PC 6 was found to be marginally significant for the effects of age and the interaction of age and IOP but was not the most parsimonious model evaluated for that PC, and PC 6 represents only a small aspect of the shape.

4. Discussion

Three main results arise from this work: first, cross-sectional human LC shape and its variations can be quantified accurately and completely using EFA and geometric morphometrics. Moreover, the statistical shape model derived from these methods enabled us to evaluate the association of LC shape with two important risk factors for glaucoma: IOP and age. Second, the mean shape of the real LCs used in our study was symmetric, although 14% of shape variation was due to superior–inferior asymmetry (PC 3). Third, this component of LC shape variation was associated with IOP; higher IOP correlating with greater curvature of the LC superiorly compared to inferiorly.

The average shape of the LC specimens in our sample was consistent with the classical description of LC morphology; posteriorly bowed centrally relative to peripherally (i.e. U-shaped) and symmetric about the central axis (Jonas et al., 2003). The major patterns of shape variation around this mean configuration represent coupled changes in LC thickness and depth (PCs 1 and 2) and account for a significant proportion of the overall variance in the shape. Comparative data on the distribution of morphological features of the LC are previously unreported in the literature, and it is thus difficult to posit a 'normal' profile of LC shape variation based on our findings. It is possible that some of the thickness variation observed may be associated with the imposed experimental conditions, as found in animal models (Fatehee et al., 2011). While little data exists describing the acute response in human eyes, there is a substantial body of evidence implicating open-angle glaucoma in structural changes of the LC. Compression, deformation and eventual thinning of the LC in glaucomatous eyes have been described in histologic and light microscopy studies (Jonas et al., 2003, 2004), and subsequently, electron microscopy has been used to document considerable thinning of the LC in eyes affected by glaucoma with the degree of thinning commensurate with disease severity (Quigley et al., 1983).

Various descriptive terms have been ascribed to LC morphology in attempts to characterize its shape, however, these predominantly relate to the anterior surface of the structure due to the difficulties associated with visualizing the posterior anatomy. Quigley et al. reported that in most ONHs the topography of the anterior LC surface is 'saddle' shaped, reflecting greater posterior bowing of the superior–inferior axis relative to the nasal–temporal axis (Quigley and Addicks, 1981). Recent work utilizing *in vivo* 3D LC images obtained by enhanced depth imaging-OCT supports this finding. Park and colleagues observed that the depth profile of the LC along the superior–inferior axis was W-shaped, indicating regional differences in the position of the LC insertion such that the

Table 1
Summary of mixed-effect models of PCs describing LC shape for various predictors.

Predictors PC	Age		IOP		Age and IOP		Age, IOP and interactions	
	AIC	*p*	AIC	*p*	AIC	*p*	AIC	*p*
1	**−42.40**	**0.96**	−40.07	0.95	−25.99	0.96	−4.79	0.88
2	**−58.67**	**0.75**	−56.52	0.17	−42.42	0.17	−19.08	0.67
3	−58.10	0.80	**−63.28**	**0.03***	−47.27	*0.03	−25.15	0.84
4	**−83.89**	**0.56**	−83.24	0.35	−66.46	0.33	−43.03	0.65
5	**−86.40**	**0.75**	−85.11	0.78	−67.82	0.77	−44.65	0.52
6	**−92.90**	**0.69**	−91.45	0.43	−74.12	0.46	−54.07	*0.04

AIC – Akaike Information Criterion; Best-fitting model for each PC is in bold text; $^{*}p < 0.05$; For Age and IOP, and Age, IOP and interactions a cell shows the smallest *p* value.

superior and inferior zones were more posteriorly located than their nasal and temporal counterparts (Park et al., 2012). In addition, Lee et al. further partition LC shape into five categories; flat, U-shaped, slope configuration, focal concavity, and W-shaped, identified in 18 (13.1%), 6 (4.4%), 16 (11.7%), 32 (23.4%), and 65 (47.4%), of their study cohort, respectively (Lee et al., 2012). This 'bowtie'-shaped horizontal central ridge corresponding to W-shaped LCs is hypothesized to represent denser connective tissue and smaller diameter LC pores, concurring with previous reports of an increased propensity for the superior and inferior ONH regions to sustain glaucomatous damage (Quigley and Addicks, 1981; Radius and Gonzales, 1981; Park et al., 2012). We did not observe this type of LC shape profile in our data. The origin of this difference remains to be determined, although it may be due to differences between OCT imaging and histology in the definition of the boundaries used to identify the LC. In our study, we selected sections that did not contain the central retinal artery or vein, which may contribute to a W-shaped profile. It is also possible that this is an effect of histological processing or the release of residual stresses (Grytz and Downs, 2012).

We found a statistically significant association between IOP and the asymmetry component of LC shape variation; increasing IOP correlates with increasing curvature of the LC superiorly and/or decreasing curvature inferiorly along the central vertical axis. Based on our data, it is impossible to determine whether the asymmetry is of significance in the pathophysiology of glaucoma. As with the quantification of 'normal' LC shape, data to characterize LC shape variation with IOP (or any other potential risk factor) is very sparse in the literature and we suspect this is primarily a result of the conceptual and methodological issues traditionally associated with the measurement of shape. Studies of the biomechanical response of the ONH have documented thinning and posterior displacement of the LC with IOP elevation (Sigal and Ethier, 2009), but effects on other morphological characteristics of the structure are less certain. More research is therefore needed to ascertain the role of LC shape variation as a pathognomonic sign for early glaucoma development. We cannot ascertain a mechanism for the vertical asymmetry observed in this work, but regional differences in ONH anatomy may have a role to play. Previous research has shown that the superior and inferior parts of the LC contain larger pores and thinner connective tissue support than the nasal and temporal sectors (Quigley and Addicks, 1981). This may translate to regional preferences in glaucomatous (neuroretinal rim) NRR loss, dependent on disease stage; for example, in early glaucoma the inferotemporal sector of the NRR is typically affected first, followed by the superotemporal region (Jonas et al., 1999). This pattern of ONH involvement may have some bearing on the observation of LC asymmetry found in the current work. Although the mean LC shape in our study was symmetric, about 14% of the sample variation was associated with asymmetry in curvature of the structure along the vertical axis. This was an unexpected finding that also highlights the power of the statistical shape model as an exploratory tool, obviating the need to define morphological features of interest *a priori*.

Historically, ocular morphometry has been done using so-called "traditional morphometrics" parameters, such as lengths, widths, angle and ratios to capture information about form. While these parameters record biologically meaningful aspects of an organism or structure, the geometrical (spatial) relationships between the anatomical landmarks among which these measurements are taken are not maintained throughout the analytical process (Sanfilippo et al., 2009). This loss of information often results in a dramatic reduction in the statistical power and ability to efficiently separate size and shape. Instead, in this work, we employed a geometric morphometrics approach. This approach has several advantages over traditional morphometrics. Among these were the ability to identify shape variations without defining them *a priori*, and the preservation of the spatial relationships between landmarks. In the geometric morphometric toolkit (e.g. Procrustes analysis, sliding semi-landmark analysis), EFA was the natural choice of technique to produce a statistical shape model of the LC. Our specimens were optimally suited to boundary outline methods of morphometric assessment. Also, in contrast with traditional morphometric methods, by using EFA it was possible to generate a graphical representation of mean shapes and study trends in shape variation.

This work has several methodological strengths, particularly in the preparation of the histologic LC sections. To ensure homology among our samples, we used sections that were geometrically accurate through the center of the LC by utilizing 3D model reconstructions of each ONH. In addition, we used an iterative scheme to label each section, thus minimizing potential artifacts from warping and uneven staining. Prior to investigating shape variation in a sample of real LCs, we validated our technique on a synthetic group of LCs with known shape characteristics applied. A useful but unexpected finding from this component of the analysis was that the synthetic LC shapes had modes of variation representative of the real specimens in our sample. This indicates that the sampling of the space specified for modeling is consistent with the distribution of human LCs, thus enabling parallel interpretation of the results. The most important limitation of this work that requires discussion is the potential that histological sections may have deformed or warped during preparation and are therefore inaccurate depictions of the morphology *in vivo*. We minimized these effects in the following ways: we embedded the tissues in JB-4 plastic, which reduces warping during sectioning; we used fiducial markers and unwarping techniques; we adopted an iterative process of segmentation to ensure that the 3D features of the reconstructed ONH were consistent with one another (Sigal et al., 2005b). We have demonstrated that our technique produces highly realistic ONH geometries that match very well with fundus images acquired before fixation and sectioning (Sigal et al., 2005b). Another obvious limitation of this study is the small sample size, but as this work was intended as an expository investigation of the potential of statistical shape models in the analysis of LC shape, the issue of larger samples can be addressed in further analyses. We should also note that, except for the donor eyes from one subject, all donors were aged over 70 years. Thus, our results on the association of age with LC shape reflect a population of relatively old people, and it is unclear whether our results extend to younger ages.

In summary, we have illustrated the power and utility of the geometric morphometric method of EFA in the mathematical characterization of LC shape. Compared to traditional methods of shape description, these tools enable visualization of patterns of shape variation and provide a statistical basis for investigating the

covariation of shape with other variables. We found that the mean LC shape was symmetrical although there was an element of variation present that may be described as superior-inferior asymmetry. Mixed-effects modeling showed an association between this component of shape and IOP, with more asymmetry at higher IOP. In this study we have laid a foundation for the successful application of statistical shape models in the analysis of ONH morphology and their integration into ocular biomechanics research. We envisage that further work will incorporate *in vivo* images from OCT to characterize the three-dimensional architecture of the neural and connective tissues of the ONH (Nadler et al., 2013; Wang et al., 2013).

Funding

National Institutes of Health (P30-EY008098 and R01-EY023966); Eye and Ear Foundation (Pittsburgh, PA); Consejo Nacional de Ciencia y Tecnologia de Mexico; Canadian Institutes for Health Research; Glaucoma Research Society of Canada. We thank the Eye Bank of Canada, Ontario Division, for providing donor tissue.

References

Claude, J., 2008. Morphometrics with R. Springer, New York, pp. 221–229.
Fatehee, N., Yu, P.K., Morgan, W.H., Cringle, S.J., Yu, D.Y., 2011. The impact of acutely elevated intraocular pressure on the porcine optic nerve head. Investig. Ophthalmol. Vis. Sci. 52, 6192–6198.
Grytz, R., Downs, J.C., 2012. A forward incremental prestressing method with application to inverse parameter estimations and eye-specific simulations of posterior scleral shells. Comput. Methods Biomech. Biomed. Eng. http://dx.doi.org/10.1080/10255842.2011.641119 (accepted in Nov 2011).
Grytz, R., Sigal, I.A., Ruberti, J.W., Meschke, G., Downs, J.C., 2012. Lamina cribrosa thickening in early glaucoma predicted by a microstructure motivated growth and remodeling approach. Mech. Mater. 44, 99–109.
Jonas, J.B., Berenshtein, E., Holbach, L., 2004. Lamina cribrosa thickness and spatial relationships between intraocular space and cerebrospinal fluid space in highly myopic eyes. Investig. Ophthalmol. Vis. Sci. 45, 2660–2665.
Jonas, J.B., Berenshtein, E., Holbach, L., 2003. Anatomic relationship between lamina cribrosa, intraocular space, and cerebrospinal fluid space. Investig. Ophthalmol. Vis. Sci. 44, 5189–5195.
Jonas, J.B., Budde, W.M., Panda-Jonas, S., 1999. Ophthalmoscopic evaluation of the optic nerve head. Surv. Ophthalmol. 43, 293–320.
Jonas, J.B., Mardin, C.Y., Schlötzer-Schrehardt, U., Naumann, G.O., 1991. Morphometry of the human lamina cribrosa surface. Investig. Ophthalmol. Vis. Sci. 32, 401–405.
Kuhl, F.P., 1982. Elliptic Fourier features of a closed contour. Comput. Graph. Image Process. 18, 236–258.
Lee, E.J., Kim, T.-W., Weinreb, R.N., Suh, M.H., Kang, M., Park, K.H., Kim, S.H., Kim, D.M., 2012. 3-Dimensional evaluation of the lamina cribrosa using spectral domain optical coherence tomography in glaucoma. Investig. Ophthalmol. Vis. Sci. 53, 198–204.
Nadler, Z., Wang, B., Wollstein, G., Nevins, J.E., Ishikawa, H., Kagemann, L., Sigal, I.A., Ferguson, R.D., Hammer, D.X., Grulkowski, I., Liu, J.J., Kraus, M.F., Lu, C.D., Hornegger, J., Fujimoto, J.G., Schuman, J.S., 2013. Automated lamina cribrosa microstructural segmentation in optical coherence tomography scans of healthy and glaucomatous eyes. Biomed. Opt. Express 4, 2596–2608.
Park, S.C., Kiumehr, S., Teng, C.C., Tello, C., Liebmann, J.M., Ritch, R., 2012. Horizontal central ridge of the lamina cribrosa and regional differences in laminar insertion in healthy subjects. Investig. Ophthalmol. Vis. Sci. 53, 1610–1616.
Quigley, H.A., Cone, F.E., 2013. Development of diagnostic and treatment strategies for glaucoma through understanding and modification of scleral and lamina cribrosa connective tissue. Cell Tissue Res. 353, 231–244.
Quigley, H.A., Brown, A.E., Morrison, J.D., Drance, S.M., 1990. The size and shape of the optic disc in normal human eyes. Arch. Ophthalmol. 108, 51–57.
Quigley, H.A., Hohman, R.M., Addicks, E.M., Massof, R.W., Green, W.R., 1983. Morphologic changes in the lamina cribrosa correlated with neural loss in open-angle glaucoma. Am. J. Ophthalmol. 95, 673–691.
Quigley, H.A., Addicks, E.M., 1981. Regional differences in the structure of the lamina cribrosa and their relation to glaucomatous optic nerve damage. Arch. Ophthalmol. 99, 137–143.
R Development Core Team, 2012. R: a Language and Environment for Statistical Computing. R Foundation for Statistical Computing, Vienna, Austria, ISBN 3-900051-07-0.
Radius, R.L., Gonzales, M., 1981. Anatomy of the lamina cribrosa in human eyes. Arch. Ophthalmol. 99, 2159–2162.
Ren, R., Wang, N., Li, B., Li, L., Gao, F., Xu, X., Jonas, J.B., 2009. Lamina cribrosa and peripapillary sclera histomorphometry in normal and advanced glaucomatous Chinese eyes with various axial length. Investig. Ophthalmol. Vis. Sci. 50, 2175–2184.
Sanfilippo, P.G., Cardini, A., Hewitt, A.W., Crowston, J.G., Mackey, D.A., 2009. Optic disc morphology – rethinking shape. Prog. Retin. Eye Res. 28, 227–248.
Sigal, I.A., Flanagan, J.G., Lathrop, K.L., Tertinegg, I., Bilonick, R., 2012. Human lamina cribrosa insertion and age. Investig. Ophthalmol. Vis. Sci. 53, 6870–6879.
Sigal, I.A., Grimm, J.L., 2012. A few good responses: which mechanical effects of IOP on the ONH to study? Investig. Ophthalmol. Vis. Sci. 53, 4270–4278.
Sigal, I.A., 2011. An applet to estimate the IOP-induced stress and strain within the optic nerve head. Investig. Ophthalmol. Vis. Sci. 52, 5497–5506.
Sigal, I.A., Flanagan, J.G., Tertinegg, I., Ethier, C.R., 2010. 3D morphometry of the human optic nerve head. Exp. Eye Res. 90, 70–80.
Sigal, I.A., Ethier, C.R., 2009. Biomechanics of the optic nerve head. Exp. Eye Res. 88, 799–807.
Sigal, I.A., Flanagan, J.G., Ethier, C.R., 2005a. Factors influencing optic nerve head biomechanics. Investig. Ophthalmol. Vis. Sci. 46, 4189–4199.
Sigal, I.A., Flanagan, J.G., Tertinegg, I., Ethier, C.R., 2005b. Reconstruction of human optic nerve heads for finite element modeling. Technol. Health Care 13, 313–329.
Sigal, I.A., Flanagan, J.G., Tertinegg, I., Ethier, C.R., 2004. Finite element modeling of optic nerve head biomechanics. Investig. Ophthalmol. Vis. Sci. 45, 4378–4387.
Wang, B., Nevins, J.E., Nadler, Z., Wollstein, G., Ishikawa, H., Bilonick, R.A., Kagemann, L., Sigal, I.A., Grulkowski, I., Liu, J.J., Kraus, M., Lu, C.D., Hornegger, J., Fujimoto, J.G., Schuman, J.S., 2013. In vivo lamina cribrosa micro-architecture in healthy and glaucomatous eyes as assessed by optical coherence tomography. Investig. Ophthalmol. Vis. Sci. 54, 8270–8274.
Yang, H., Downs, J.C., Sigal, I.A., Roberts, M.D., Thompson, H., Burgoyne, C.F., 2009. Deformation of the normal monkey optic nerve head connective tissue after acute IOP elevation within 3-D histomorphometric reconstructions. Investig. Ophthalmol. Vis. Sci. 50, 5785–5799.
Yang, H., Downs, J.C., Girkin, C.A., Sakata, L., Bellezza, A., Thompson, H., Burgoyne, C.F., 2007. 3-D histomorphometry of the normal and early glaucomatous monkey optic nerve head: lamina cribrosa and peripapillary scleral position and thickness. Investig. Ophthalmol. Vis. Sci. 48, 4597–4607.